Non-Local Means Methods Using CT Side Information for I-131 SPECT Image Reconstruction

Se Young Chun, *Member, IEEE,* Jeffrey A. Fessler, *Fellow, IEEE,* and Yuni K. Dewaraja, *Member, IEEE*

***Abstract*—Recently, non-local means (NLM) methods for both image denoising and inverse problems have shown promising results in image processing and medical imaging. Moreover, some researchers have also shown that using additional information with low noise and/or high resolution for these problems can improve the image quality further. We investigated several NLM methods including NLM filters and NLM regularizers with and without CT side information for I-131 SPECT image reconstruction. We compared two different ways to incorporate CT side information in the NLM filtering methods. We also propose a new way of incorporating side information in the NLM reconstruction method. XCAT simulation results with two uniform tumors (72 cc, 11 cc) show that the NLM filtering method with CT side information decreased the root mean square error (RMSE) up to 18.6% as compared to unregularized method. Our proposed NLM-based regularizers in iterative image reconstructions with CT side information also yielded up to 29.2% better RMSE and up to 18.1% better recovery coefficient than unregularized reconstruction.**

I. Introduction

NON-LOCAL means (NLM) methods exploit the self-similarity of small patches in an image for denoising [1] and for regularization [2]. These methods yield superior denoising results as compared to conventional local filters such as a Gaussian filter. Moreover, some researchers have also shown that using these NLM methods with high-quality side information can improve the image quality further [3]–[7]. Multi-modal imaging systems such as PET-CT, PET-MR, or SPECT-CT can benefit from these state-of-the-art methods to reconstruct better-quality images.

SPECT-based dosimetry in I-131 radioimmunotherapy and radioiodine therapy can be a natural application for these NLM methods using additional side information since high resolution CT image is available from SPECT-CT system. Improved accuracy in SPECT quantification for both total activity and distribution using these methods can potentially improve dose-response correlations so that the efficacy and toxicity of treatments can be better-assessed.

In this paper, we evaluate various NLM filters and reconstruction methods with and without side information for an I-131 SPECT-CT system, and compare the results with that of conventional ordered-subset expectation-maximization (OSEM) [8] with and without Gaussian post-reconstruction smoothing. We also propose a new way of incorporating side information in the NLM methods and show some promising preliminary results. 3D XCAT phantom simulation was performed to evaluate NLM post-reconstruction filtering and NLM reconstruction methods with and without high-resolution CT information.

This work was supported in part by NIH grant 2RO1 EB001994.

S Y Chun is with the Department of Electrical Engineering and Computer Science and with the Department of Radiology, University of Michigan, Ann Arbor, MI 48109 USA (delight@umich.edu).

J A Fessler is with the Department of Electrical Engineering and Computer Science, University of Michigan, Ann Arbor, MI 48109 USA (fessler@umich.edu).

Y K Dewaraja is with the Department of Radiology, University of Michigan, Ann Arbor, MI 48109 USA (yuni@umich.edu).

II. Method

A. Statistical image reconstruction for SPECT

The SPECT image $\boldsymbol{x}$ can be reconstructed iteratively from

$$\hat{\boldsymbol{x}} \triangleq \underset{\boldsymbol{x} \geq \boldsymbol{0}}{\operatorname{argmin}} \, \mathrm{L}(\boldsymbol{y}|\boldsymbol{x}) \tag{1}$$

where $\boldsymbol{y}$ is a measured sinogram data, L denotes a negative Poisson log-likelihood function

$$\mathrm{L}(\boldsymbol{y}|\boldsymbol{x}) = \sum_i \bar{y}_i(\boldsymbol{x}) - y_i \log \bar{y}_i(\boldsymbol{x}), \tag{2}$$

y_i is the ith element of the measurement $\boldsymbol{y}$,

$$\bar{y}_i(\boldsymbol{x}) \triangleq [\boldsymbol{A}\boldsymbol{x}]_i + s_i,$$

and $\boldsymbol{A}$ denotes the system model and s_i is a scatter component for the ith measurement. We incorporated the attenuation maps from the CT data and the full collimator-detector response including penetration tails [9] in the matrix $\boldsymbol{A}$. We assumed known s_i. Equation (1) can be solved using algorithms such as OSEM [8].

Unregularized image reconstruction in (1) is *ill-posed*. Even though more iteration is required for reconstructing high-frequency information, more iteration also amplifies noise. One can stop iterations before convergence to obtain image without much noise or one can use post-reconstruction filters such as Gaussian filter to reduce the noise. However, Gaussian filtering also reduces image details.

B. NLM filtering with side information

Given the reconstructed noisy SPECT image $\hat{\boldsymbol{x}}$, the conventional NLM filtered image at the ith voxel can be defined as follows [1]:

$$[\hat{\boldsymbol{x}}_{\mathrm{NLM}}]_i = \sum_j \frac{w_{\mathrm{f}}(i,j|\hat{\boldsymbol{x}})}{\sum_{j'} w_{\mathrm{f}}(i,j'|\hat{\boldsymbol{x}})} [\hat{\boldsymbol{x}}]_j \tag{3}$$

where $w_{\mathrm{f}}(i,j|\boldsymbol{x}) \triangleq \exp\left(-\|\boldsymbol{N}_i\boldsymbol{x} - \boldsymbol{N}_j\boldsymbol{x}\|^2/(2\sigma_{\mathrm{f}}^2 N_{\mathrm{f}})\right)$, $\boldsymbol{N}_j\boldsymbol{x}$ is the patch of $\boldsymbol{x}$ centered at the jth voxel, σ_{f} is a design parameter, and N_{f} is the number of voxels in the patch.

When anatomical side information is incorporated into NLM filtering, a usual form is [3], [5]

$$[\hat{\boldsymbol{x}}_{\mathrm{NLMCT1}}]_i = \sum_j \frac{w_{\mathrm{f}}(i,j|\hat{\boldsymbol{x}}) w_{\mathrm{a}}(i,j|\boldsymbol{g})}{\sum_{j'} w_{\mathrm{f}}(i,j'|\hat{\boldsymbol{x}}) w_{\mathrm{a}}(i,j'|\boldsymbol{g})} [\hat{\boldsymbol{x}}]_j \quad (4)$$

where

$$w_{\mathrm{a}}(i,j|\boldsymbol{g}) \triangleq \exp\left(-\frac{\|\boldsymbol{M}_i\boldsymbol{g} - \boldsymbol{M}_j\boldsymbol{g}\|^2}{2\sigma_{\mathrm{a}}^2 N_{\mathrm{a}}}\right),$$

$\boldsymbol{g}$ is an anatomical CT image, $\boldsymbol{M}_j\boldsymbol{g}$ is the patch of $\boldsymbol{g}$ centered at the jth voxel, σ_{a} is another design parameter to determine the performance of the filter, and N_{a} is the number of voxels in the patch $\boldsymbol{M}_j\boldsymbol{g}$.

We propose to use another form of incorporating side information in NLM filtering as follows:

$$[\hat{\boldsymbol{x}}_{\mathrm{NLMCT2}}]_i = \sum_j \frac{w_{\mathrm{f}}(i,j|\hat{\boldsymbol{x}}) + \tau w_{\mathrm{a}}(i,j|\boldsymbol{g})}{\sum_{j'} w_{\mathrm{f}}(i,j'|\hat{\boldsymbol{x}}) + \tau w_{\mathrm{a}}(i,j'|\boldsymbol{g})} [\hat{\boldsymbol{x}}]_j. \quad (5)$$

If we can trust the anatomical information more than the emission information (*e.g.*, high correlation between anatomical and emission information, high noise in emission data), we can use large τ and vice versa. We set $\tau = 1$ for simplicity in our simulations.

In (4), if the anatomical side information patches are very different (*i.e.*, $w_{\mathrm{a}} \approx 0$), then that pixel would not be used for filtering even though the SPECT patches are very similar (*i.e.*, $w_{\mathrm{f}} \approx 1$). In other words, (4) trusts anatomical side information more than noisy emission information. Many methods including Bowsher prior fall into this category [3], [5], [6], [10]. For example, for Bowsher prior, we need to re-define the weight w_{a} as follows: $w_{\mathrm{a}}(i,j) = 1$ if $\|\boldsymbol{M}_i\boldsymbol{g} - \boldsymbol{M}_j\boldsymbol{g}\| < \sigma_{\mathrm{a}}(i)$ and $w_{\mathrm{a}}(i,j) = 0$ otherwise. $\sigma_{\mathrm{a}}(i)$ is a spatially-varying value such that $\sum_j w_{\mathrm{a}}(i,j)$ is a fixed constant.

In (5), even if the anatomical side information patches are very different (*i.e.*, $w_{\mathrm{a}} \approx 0$), the weight for that pixel will not be zero when the SPECT patches are very similar (*i.e.*, $w_{\mathrm{f}} + w_{\mathrm{a}} \approx 1$). That is to say, (5) trusts both anatomical CT side information and emission information. There are some methods that implement this principle with different forms [4], [7]. The former combines emission and anatomical information before applying nonlinear exponential function, and the latter combines them after.

C. NLM reconstruction with side information

One can incorporate NLM methods into iterative image reconstruction. NLM weights for NLM filtering can be easily calculated using given noisy images, but NLM weights for NLM reconstruction usually have been computed from the initial image, which may be inaccurate, or updated iteratively using intermediate images, which may change the cost function [2].

Recently, Yang and Jacob proposed a generalized NLM regularization framework [11] as follows:

$$\hat{\boldsymbol{x}} \triangleq \underset{\boldsymbol{x}\geq\boldsymbol{0}}{\operatorname{argmin}} \mathrm{L}(\boldsymbol{y}|\boldsymbol{x}) + \beta \mathrm{R}_{\mathrm{NLM}}(\boldsymbol{x}) \quad (6)$$

where β is a regularization parameter and

$$\mathrm{R}_{\mathrm{NLM}}(\boldsymbol{x}) \triangleq \sum_{i,j} (1 - w_{\mathrm{f}}(i,j|\boldsymbol{x})). \quad (7)$$

They showed that a surrogate function for (7) has a similar form to NLM filtering in (3). The gradient $\nabla \mathrm{R}_{\mathrm{NLM}}(\boldsymbol{x}^{(n)})$ of this regularizer (7) shows this NLM form:

$$\sum_{i,j} \frac{w_{\mathrm{f}}(i,j|\boldsymbol{x}^{(n)})}{N_{\mathrm{f}}\sigma_{\mathrm{f}}^2} (\boldsymbol{N}_i - \boldsymbol{N}_j)'(\boldsymbol{N}_i - \boldsymbol{N}_j)\boldsymbol{x}^{(n)}. \quad (8)$$

Note that a usual NLM regularizer [2]

$$\sum_{i,j} \frac{w_{\mathrm{f}}(i,j|\boldsymbol{x}^{(n)})}{2N_{\mathrm{f}}\sigma_{\mathrm{f}}^2} \|\boldsymbol{N}_i\boldsymbol{x} - \boldsymbol{N}_j\boldsymbol{x}\|^2$$

has also the same gradient (8) as that of (7) at $\boldsymbol{x}^{(n)}$.

Inspired by [11], we designed two different NLM regularizers to incorporate anatomical side information corresponding to (4) and (5), respectively. One regularizer that is similar to (4) is

$$\mathrm{R}_{\mathrm{NLMCT1}}(\boldsymbol{x}|\boldsymbol{g}) \triangleq \sum_{i,j} w_{\mathrm{a}}(i,j|\boldsymbol{g})(1 - w_{\mathrm{f}}(i,j|\boldsymbol{x})) \quad (9)$$

and the gradient of (9) at $\boldsymbol{x}^{(n)}$ is

$$\sum_{i,j} \frac{w_{\mathrm{a}}(i,j|\boldsymbol{g}) w_{\mathrm{f}}(i,j|\boldsymbol{x}^{(n)})}{N_{\mathrm{f}}\sigma_{\mathrm{f}}^2} (\boldsymbol{N}_i - \boldsymbol{N}_j)'(\boldsymbol{N}_i - \boldsymbol{N}_j)\boldsymbol{x}^{(n)}.$$

Bowsher prior and similar methods fall into this category [6], [10].

We propose to use the following regularizer that is similar to (5):

$$\begin{aligned} &\mathrm{R}_{\mathrm{NLMCT2}}(\boldsymbol{x}|\boldsymbol{g}) \quad (10)\\ &\triangleq \sum_{i,j} (1 - w_{\mathrm{f}}(i,j|\boldsymbol{x})) - \tau w_{\mathrm{a}}(i,j|\boldsymbol{g}) \log w_{\mathrm{f}}(i,j|\boldsymbol{x}) \\ &= \sum_{i,j} (1 - w_{\mathrm{f}}(i,j|\boldsymbol{x})) + \frac{\tau w_{\mathrm{a}}(i,j|\boldsymbol{g})}{2\sigma_{\mathrm{f}}^2 N_{\mathrm{f}}} \|\boldsymbol{N}_i\boldsymbol{x} - \boldsymbol{N}_j\boldsymbol{x}\|^2 \end{aligned}$$

and the gradient of (10) at $\boldsymbol{x}^{(n)}$ is

$$\sum_{i,j} \frac{w_{\mathrm{f}}(i,j|\boldsymbol{x}^{(n)}) + \tau w_{\mathrm{a}}(i,j|\boldsymbol{g})}{N_{\mathrm{f}}\sigma_{\mathrm{f}}^2} (\boldsymbol{N}_i - \boldsymbol{N}_j)'(\boldsymbol{N}_i - \boldsymbol{N}_j)\boldsymbol{x}^{(n)}.$$

Even though [4] and [7] implemented the similar principle of (5) as (10), the resulting regularizer (10) is very different from the regularizers in [4], [7]. For very similar anatomical side information patches (*i.e.*, $w_{\mathrm{a}} \approx 1$), our proposed regularizer strongly minimize the difference between two corresponding patches of emission image by using l_2 norm $w_{\mathrm{a}}(i,j|\boldsymbol{g})\|\boldsymbol{N}_i\boldsymbol{x} - \boldsymbol{N}_j\boldsymbol{x}\|^2$.

We used L-BFGS-B algorithm with non-negativity constraints [12] to reconstruct the image by minimizing the penalized-likelihood cost function (6).

III. Simulation results

We simulated a 3D SPECT-CT system with the attenuation map, collimator-detector response, and scatter component (128×21, 4.8^2mm^2 pixel size). We used the XCAT phantom [13] to generate the true SPECT and CT images as shown in Fig. 1. The activities of different organs and the size of tumors in SPECT image were determined based on a patient data in [14] for more realistic simulation. The

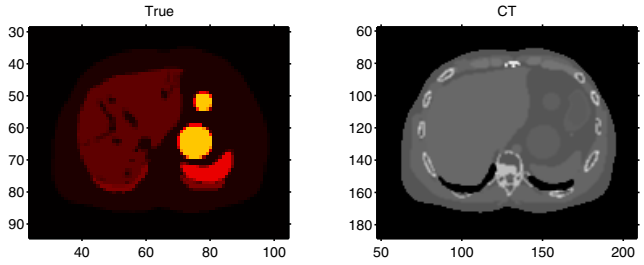

(a) SPECT TRUE (b) CT TRUE

Fig. 1. True SPECT and CT images of 3D XCAT phantom with two spherical uniform tumors (72 cc, 11 cc).

dimensions of the SPECT and CT images were $128 \times 128 \times 21$, 4.8^3mm^3 voxel size and $256 \times 256 \times 42$, 2.4^3mm^3 voxel size, respectively. We placed two spherical uniform tumors with the size of 72 cc and 11 cc in both SPECT and CT images. We generated projection data using the system matrix that incorporates the attenuation maps and full collimator-detector response including penetration tails [9]. After adjusting the total count number to be similar to the total count number in a patient data, we added a Poisson noise.

We evaluated the reconstructed image quality using the root mean squared error (RMSE) between the true and the reconstructed image and using the recovery coefficient (RC) for two spherical lesions (ROI) defined as follows:

$$\text{RC} \triangleq \frac{\text{count in ROI (recon)}}{\text{count in FOV (recon)}} \times \frac{\text{count in FOV (true)}}{\text{count in ROI (true)}}.$$

First, we reconstructed images using conventional OSEM (up to 100 iterations with 6 subsets). Fig. 2 shows the reconstructed images at different iterations and the RMSE and RC over iterations. In Fig. 2 (a) and (b), the OSEM reconstructed image at higher iteration contains higher contrast and higher noise. We can observe this trade-off in Fig. 2 (c). The RMSE value decreases at lower iterations since increasing contrast and detail is dominant over increasing noise, but the RMSE value increases at higher iterations (after 44 iteration) since increasing noise is dominant over increasing contrast and detail. However, Fig. 2 (d) shows that the RC increases over iteration since the definition of RC contains the averaging over ROI so that the influence of noise decreases. These quantitative values are shown in Table I.

We improved SPECT image quality using various post-reconstruction filters with and without CT side information. We applied Gaussian filter, NLM filter (3), modified NLM filters (for incorporating CT information) (4) and (5) to OSEM reconstructed images (44 and 100 iterations). Filter parameters

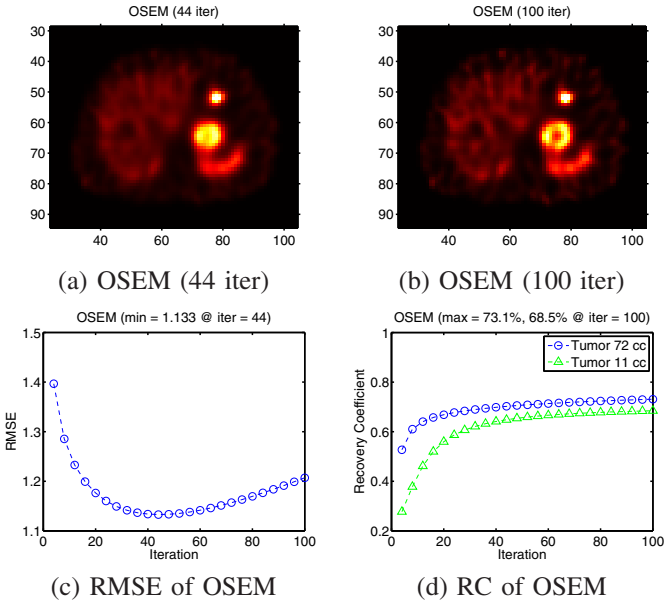

(a) OSEM (44 iter) (b) OSEM (100 iter)

(c) RMSE of OSEM (d) RC of OSEM

Fig. 2. In (a) and (b), the OSEM reconstructed image at higher iteration contains higher contrast and higher noise. In (c), RMSE value decreases at lower iterations since increasing contrast and detail is dominant over increasing noise, but RMSE value increases at higher iterations since the latter is dominant over the former. In (d), RC increases over iteration since the averaging effect of RC reduced the influence of noise.

TABLE I
Quantification results: RMSE for the whole image, RC for the tumors with the size of 72 cc and 11 cc.

Method	RMSE	RC (72 cc)	RC (11 cc)
OSEM @ 44 iter	**1.13**	70.2%	64.8%
OSEM @ 100 iter	1.21	**73.1%**	**68.5%**
Gaussian filter @ 44 iter	1.06	68.8%	59.3%
Gaussian filter @ 100 iter	1.04	68.8%	56.4%
NLM filter @ 44 iter	1.05	70.4%	65.2%
NLM filter @ 100 iter	**1.02**	**73.6%**	**68.8%**
NLM CT1 filter	0.97	71.1%	63.4%
NLM CT2 filter	**0.92**	**74.1%**	65.9%
NLM recon	0.98	**79.2%**	**77.8%**
NLM CT1 recon	1.00	83.7%	72.7%
NLM CT2 recon	**0.80**	**86.3%**	**80.8%**

were chosen to yield best RMSE value using greedy algorithm. Fig. 3 shows various post-reconstruction filtered images with and without CT side information. NLM CT2 filter in Fig. 3 (f) yielded the closest image to the true image visually. Table I also shows that NLM filtering yielded 9.7 % better RMSE than unregularized reconstruction and that filtering with CT side information yielded 18.6 % better RMSE than unregularized method. However, RC did not change much with and without filtering since the definition of RC contains the averaging over ROI and this averaging reduced noise like filtering. Thus, RC with unregularized reconstruction also yielded comparable RC results.

NLM reconstruction with and without CT side information improved SPECT image quality significantly. We applied NLM regularizer (7), modified NLM regularizers with CT side information (9) and (10) in the reconstruction (6). We chose various parameters to yield the best RMSE using greedy algorithm and ran 100 iterations. Fig. 4 show the reconstructed

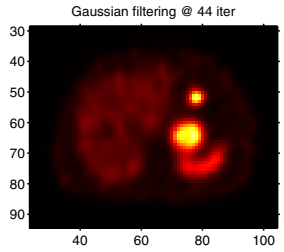

(a) Gaussian filter @ 44 iter

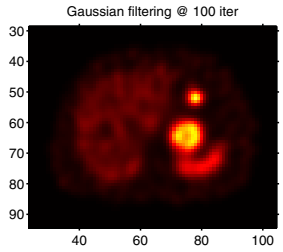

(b) Gaussian filter @ 100 iter

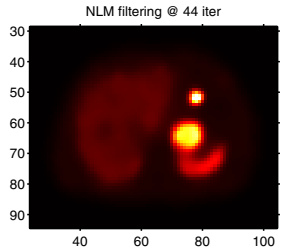

(c) NLM filter @ 44 iter

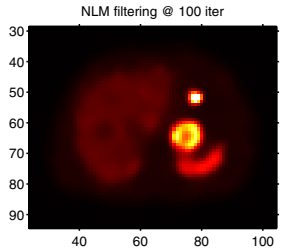

(d) NLM filter @ 100 iter

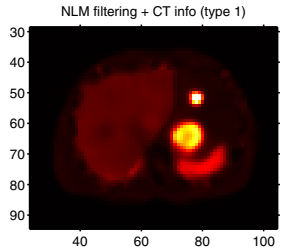

(e) NLM CT1 filter

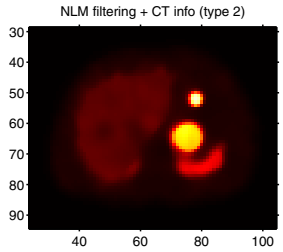

(f) NLM CT2 filter

Fig. 3. Images using various post-reconstruction filters with and without CT side information. Filter parameters were chosen to yield best RMSE value. NLM CT2 filter (f) yielded the closest image to the true image visually.

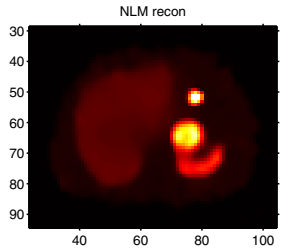

(a) NLM reconstruction

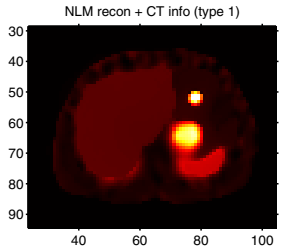

(b) NLM CT1 reconstruction

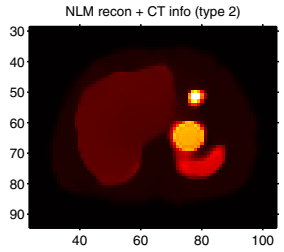

(c) NLM CT2 reconstruction

Fig. 4. Reconstructed images using three different NLM-type regularizers with and without CT side information.

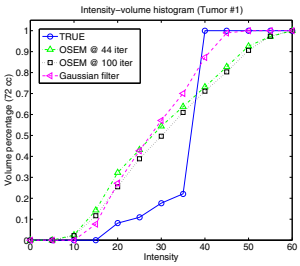

(a) unregularized OSEM

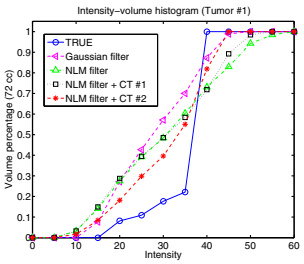

(b) NLM filters

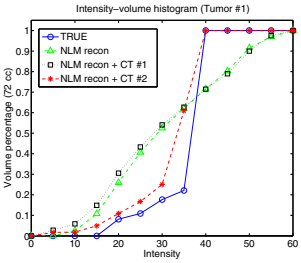

(c) NLM regularizers

Fig. 5. Intensity-Volume histogram (Tumor #1).

images using these three regularizers. The difference among these images can be clearly observed quantitatively in Table I. NLM reconstruction without CT yielded 13.3 % better RMSE than unregularized OSEM (at 44 iter) and yielded up to 13.6 % better RC than unregularized OSEM (at 100 iter). NLM reconstruction with CT side information yielded 29.2 % better RMSE than unregularized OSEM (at 44 iter) and yielded up to 18.1 % better RC than unregularized reconstruction (at 100 iter).

We compared various reconstructed and post-reconstruction filtered images by plotting intensity-volume histogram. Fig. 5 shows that using CT information for both filtering and regularizer yielded closer cumulative intensity-volume histogram to the truth. NLM CT2 regularizer (10) yielded the closest cumulative intensity-volume histogram to the truth among all compared methods.

IV. Conclusion

We compared various NLM-type filters and regularizers that use CT side information and proposed a new NLM-type regularizer using CT information. We showed that our proposed regularizer yielded superior performance in terms of RMSE, RC, and intensity-volume histogram. Further investigation is necessary such as evaluating these methods in measured phantom studies and patient studies.

References

[1] A. Buades, B. Coll, and J. M. Morel, "A review of image denoising methods, with a new one," *SIAM Multiscale Modeling and Simulation*, vol. 4, no. 2, pp. 490–530, 2005.

[2] X. Zhang, M. Burger, X. Bresson, and S. Osher, "Bregmanized nonlocal regularization for deconvolution and sparse reconstruction," *SIAM J. Imaging Sci.*, vol. 3, no. 3, pp. 253–76, 2010.

[3] C.-A. Deledalle, F. Tupin, and L. Denis, "Poisson NL means: Unsupervised non local means for poisson noise," in *2010 17th IEEE Intl. Conf. Image Proc.*, sept. 2010, pp. 801 –804.

[4] F. Rousseau, "A non-local approach for image super-resolution using intermodality priors," *Med. Im. Anal.*, vol. 14, no. 4, pp. 594–605, Aug. 2010.

[5] C. Chan, R. R. Fulton, D. D. Feng, and S. R. Meikle, "Median non-local means filtering for low SNR image denoising: Application to PET with anatomical knowledge," in *Proc. IEEE Nuc. Sci. Symp. Med. Im. Conf.*, 2010, pp. 3613–8.
[6] K. Vunckx, A. Atre, K. Baete, A. Reilhac, C. Deroose, K. V. Laere, and J. Nuyts, "Evaluation of three mri-based anatomical priors for quantitative pet brain imaging," *IEEE Trans. Med. Imaging*, vol. 31, no. 3, pp. 599–612, 2012.
[7] V.-G. Nguyen and S.-J. Lee, "Anatomy-based PET image reconstruction using nonlocal regularization," in *Proc. SPIE Medical Imaging 2012: Phys. Med. Im.*, 2012.
[8] H. M. Hudson and R. S. Larkin, "Accelerated image reconstruction using ordered subsets of projection data," *IEEE Trans. Med. Imag.*, vol. 13, no. 4, pp. 601–9, Dec. 1994.
[9] S. Chun, J. Fessler, and Y. Dewaraja, "Correction for collimator-detector response in SPECT using point spread function template," *IEEE Trans. Med. Imaging*, 2012, to appear.
[10] J. Bowsher, H. Yuan, L. Hedlund, T. Turkington, G. Akabani, A. Badea, W. Kurylo, C. Wheeler, G. Cofer, M. Dewhirst, and G. Johnson, "Utilizing MRI information to estimate F18-FDG distributions in rat flank tumors," in *Proc. IEEE Nuc. Sci. Symp. Med. Im. Conf.*, vol. 4, oct. 2004, pp. 2488 – 2492.
[11] Z. Yang and M. Jacob, "A unified energy minimization framework for nonlocal regularization," in *Proc. IEEE Intl. Symp. Biomed. Imag.*, 2011, pp. 1150–3.
[12] J. L. Morales and J. Nocedal, "Remark on "algorithm 778: L-BFGS-B: Fortran subroutines for large-scale bound constrained optimization"," *ACM Trans. Math. Softw.*, vol. 38, no. 1, pp. 7:1–7:4, Nov. 2011.
[13] W. P. Segars, M. Mahesh, T. J. Beck, E. C. Frey, and B. M. W. Tsui, "Realistic CT simulation using the 4D XCAT phantom," *Med. Phys.*, vol. 35, no. 8, pp. 3800–8, Aug. 2008.
[14] Y. K. Dewaraja, S. J. Wilderman, M. Ljungberg, K. F. Koral, K. Zasadny, and M. S. Kaminiski, "Accurate dosimetry in 131I radionuclide therapy using patient-specific, 3-dimensional methods for SPECT reconstruction and absorbed dose calculation," *Journal of Nuclear Medicine*, vol. 46, no. 5, pp. 840–849, 2005.